Title
Neutron Stars, Strange Stars, and the Nuclear Equation of State

Authors
Weber, F.
Glendenning, N.K.

Publication Date
1992-11-02

LBL-33066
UC-413

Lawrence Berkeley Laboratory
UNIVERSITY OF CALIFORNIA

Presented at the First Symposium on Nuclear Physics in the Universe, Oak Ridge, TN, September 24–26, 1992, and to appear in the Journal of Physics

Neutron Stars, Strange Stars, and the Nuclear Equation of State

F. Weber and N.K. Glendenning

November 1992

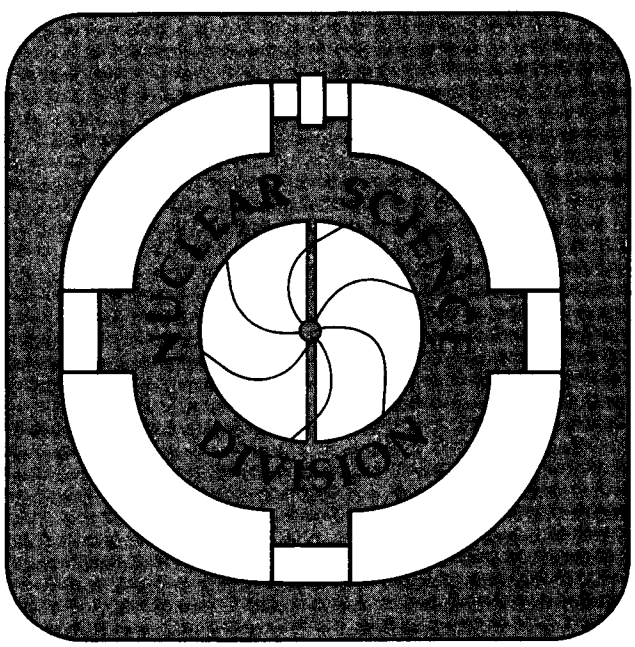

Prepared for the U.S. Department of Energy under Contract Number DE-AC03-76SF00098

DISCLAIMER

LBL - 33066

Neutron Stars, Strange Stars, and the Nuclear Equation of State*

F. Weber† and N. K. Glendenning

Nuclear Science Division
Lawrence Berkeley Laboratory
University of California
Berkeley, California 94720, U.S.A.

November 2, 1992

Presented at the
FIRST SYMPOSIUM ON NUCLEAR PHYSICS IN THE UNIVERSE
Oak Ridge, Tennessee, USA
September 24–26, 1992
To appear in The Journal of Physics

*This work was supported by the Director, Office of Energy Research, Office of High Energy and Nuclear Physics, Division of Nuclear Physics, of the U.S. Department of Energy under Contract DE-AC03-76SF00098, and the Deutsche Forschungsgemeinschaft.

†Home institute: Institute for Theoretical Physics, University of Munich, Theresienstrasse 37/III, W-8000 Munich 2, Federal Republic of Germany.

Contents

Neutron Stars, Strange Stars, and the Nuclear Equation of State

F Weber Institute for Theoretical Physics, University of Munich, Theresienstr. 37/III, W-8000 Munich 2, FRG

N K Glendenning Nuclear Science Division, Lawrence Berkeley Laboratory, University of California, Berkeley, California 94720, USA

Abstract. This article consists of three parts. In part one we review the present status of dense nuclear matter calculations, and introduce a representative collection of realistic nuclear equations of state which are derived for different assumptions about the physical behavior of dense matter (baryon population, pion condensation, possible transition of baryon matter to quark matter). In part two we review recently performed non-rotating and rotating compact star calculations performed for these equations of state. The minimum stable rotational periods of compact stars, whose knowledge is of decisive importance for the interpretation of rapidly rotating pulsars, are determined. For this purpose two different limits on stable rotation are studied: rotation at the general relativistic Kepler period (below which mass shedding at the star's equator sets in), and, secondly, rotation at the gravitational radiation-reaction instability (at which emission of gravitational waves set in which slows the star down). Part three of this article deals with the properties of hypothetical strange stars. Specifically we investigate the amount of nuclear solid crust that can be carried by a rotating strange star, and answer the question whether such objects can give rise to the observed phenomena of pulsar glitches, which is at the present time the only astrophysical test of the strange-quark-matter hypothesis.

1 Introduction

Neutron stars contain matter in one of the densest forms found in the universe. Matter in their cores possesses densities ranging from a few times ϱ_0 to an order of magnitude higher. Here $\varrho_0 = 0.15$ nucleons/fm^3 denotes the density of normal nuclear matter, which corresponds to a mass density of 2.5×10^{14} g/cm^3. The number of baryons

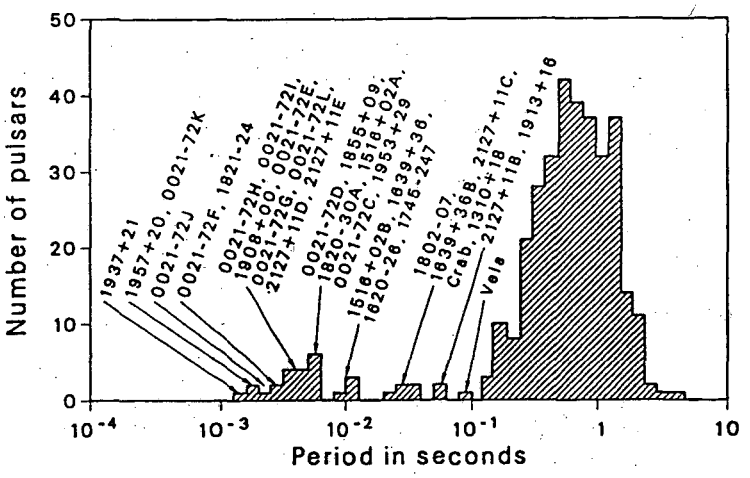

Figure 1: Distribution of pulsar periods. There is a relatively strong attenuation in sensitivity of radio pulsar surveys for periods below about 1ms [4] which is due to the fact that most pulsar surveys had no sensitivity below about 4 ms. Therefore the cut-off at short periods is possibly an artifact.

forming a neutron star is of the order of $A \approx 10^{57}$. The understanding of matter under such extreme conditions of density is one of the central but also most complex problems of physics.

Neutron stars are associated with two classes of astrophysical objects: *Pulsars* [1], which are generally accepted to be rotating neutron stars (the fastest so far observed ones have rotational periods $P \geq 1.6$ ms), and *compact X-ray sources* (e.g. Her X-1 and Vela X-1), certain of which are neutron stars in close binary orbits with an ordinary star. The first millisecond pulsar was discovered in 1982 [2], and in the next seven years about one a year has been found. The situation has changed radically with the recent discovery of an anomalously large population of millisecond pulsars in globular clusters [3], where the density of stars is roughly 1000 times that in the field of the galaxy and which are therefore very favorable environments for the formation of rapidly rotating pulsars that have been spun up by means of mass accretion from a binary companion. The distribution of the presently known pulsars as a function of their rotational period is shown in Figure 1.

As just outlined, neutron stars are objects of highly compressed matter so that the geometry of space-time is changed considerably from flat space. Thus for the construction of realistic models of rapidly rotating compact stars one has to resort to Einstein's theory of general relativity. To date only a few authors have constructed star models within this framework that are unrestricted with respect to the strength of the gravitational field of the star, not limited to small rotational star frequencies, and performed for realistic models for the equation of state. Studies fulfilling these conditions have been presented by Friedman, Ipser and Parker [5, 6], Lattimer, Prakash, Masak and Yahil [7], and Weber and Glendenning [8, 9, 10]. The studies of the latter authors are reviewed here. The equation of state of the star matter, i.e. pressure as a function of energy density, is the basic input quantity whose knowledge

over a broad range of densities (ranging from the density of iron at the star's surface up to ~ 15 times the density of normal nuclear matter reached in the cores of massive stars) is necessary in order to solve the Einstein equations. Unfortunately the physical behavior of matter under such extreme densities as in the cores of massive stars is rather uncertain and the associated equation of state is only poorly known. The models derived for it differ considerably with respect to the dependence of pressure on density, which has its origin in various sources. To mention several are: (1) the many-body technique used to determine the equation of state, (2) the model for the nucleon-nucleon interaction, (3) description of electrically charge neutral neutron star matter in terms of either (a) only neutrons, (b) neutrons and protons in β-equilibrium with electrons and muons, or (c) nucleons, hyperons and more massive baryon states in β-equilibrium with leptons, (4) inclusion of pion condensation, and (5) treatment of the transition of confined hadronic matter into quark matter. It is the purpose of this work to

- outline the present status of dense matter calculations,
- explore the compatibility of the properties of non-rotating and rotating compact star models, which are constructed for a collection of equations of state which accounts for items (1)-(5) from above, with observed data, and
- investigate the properties of strange stars [11, 12, 13] (specifically we answer the question whether such objects can give rise to the observed phenomena of pulsar glitches, which is at the present time the only astrophysical test of the strange-quark-matter hypothesis).

2 The nuclear equation of state

2.1 Theoretical framework

2.1.1 Non-relativistic approach

For non-relativistic models, the starting point is a phenomenological nucleon-nucleon interaction. In the case of the equations of state reported here, different two-nucleon potentials (denoted V_{ij}) which fit nucleon-nucleon scattering data and deuteron properties have been employed. Most of these two-nucleon potentials are supplemented with three-nucleon interactions (denoted V_{ijk}). The Hamiltonian is of the form

$$H = \sum_i \left(\frac{-\hbar^2}{2m}\right) \nabla_i^2 + \sum_{i<j} V_{ij} + \sum_{i<j<k} V_{ijk} \ . \tag{1}$$

The many-body method adopted to solve the Schroedinger equation is based on the variational approach [14, 15, 16] where a variational trial function $|\Psi_v>$ is constructed from a symmetrized product of two-body correlation operators (F_{ij}) acting on an unperturbed ground-state, i.e.

$$|\Psi_v> = \left[\hat{S} \prod_{i<j} F_{ij}\right] |\Phi> \ , \tag{2}$$

where $|\Phi>$ denotes the antisymmetrized Fermi-gas wave function,

$$|\Phi> = \hat{A} \prod_j \exp(i \boldsymbol{p}_j \cdot \boldsymbol{x}_j) \ . \tag{3}$$

The correlation operator contains variational parameters which are varied to minimize the energy per baryon for a given density ϱ (see Refs. [14, 15, 16, 17] for details):

$$E_v(\varrho) = \min \left\{ \frac{< \Psi_v | H | \Psi_v >}{< \Psi_v | \Psi_v >} \right\} \geq E_0 \ . \tag{4}$$

As indicated, E_v constitutes an upper bound to the ground-state energy E_0. The energy density $\epsilon(\varrho)$ and pressure $P(\varrho)$ are obtained from Eq. (4) by

$$\epsilon(\varrho) = \varrho \, [E_v(\varrho) + m] \ , \qquad P(\varrho) = \varrho^2 \frac{\partial}{\partial \varrho} E_v(\varrho) \ , \tag{5}$$

which leads to the equation of state in the form $P(\epsilon)$ used for the star structure calculations here.

2.1.2 Relativistic approach

A consistent theoretical framework for deriving relativistic models for the equation of state, which allows for the incorporation of dynamical two-particle correlations, is the Martin-Schwinger hierarchy of coupled Green's functions [18, 19, 20]. In the lowest order, the Martin-Schwinger hierarchy can be truncated by factorizing the four-point Green's function $g_2(1,2;1'2')$ (unprimed (primed) arguments refer to ingoing (outgoing) particles) into a product of two-point Green's functions g [$\equiv g_1(1';1')$]. This leads to the well-known relativistic *Hartree* (i.e. mean-field) and *Hartree-Fock* approximations (see Fig. 2). The *T-matrix* approximation (also known as Λ or ladder approximation), which goes beyond this, truncates the Martin-Schwinger hierarchy by factorizing the six-point Green's function $g_3(123;1'2'3')$ into products of four- and two-point functions by which dynamical two-particle correlations in matter - which are connected with the two-body potential (denoted v) - are taken into account. The main problem which one encounters hereby is the calculation of the effective scattering matrix (effective two-particle potential) in matter, T, which satisfies

$$T = v - v^{\mathrm{ex}} + \int v \, \Lambda \, T \ . \tag{6}$$

We have restricted ourselves to the so-called Λ^{00} approximation, for which the nucleon-nucleon propagator is given by the product of two free two-point Green's functions (denoted g^0), i.e. $\Lambda = i g^0 g^0$. The basic input quantity in Eq. (6) is the nucleon-nucleon interaction in free space as derived, for example, in the Bonn meson-exchange model [21]. We have adopted the latest version of this interaction together with the HEA potential [22] to compute the T matrix in neutron matter up to two-times nuclear matter density [8]. The important feature of such meson-exchange models is that the potential parameters are adjusted to the two-body nucleon-nucleon scattering data and the properties of the deuteron, whereby (in this sense) a parameter-free

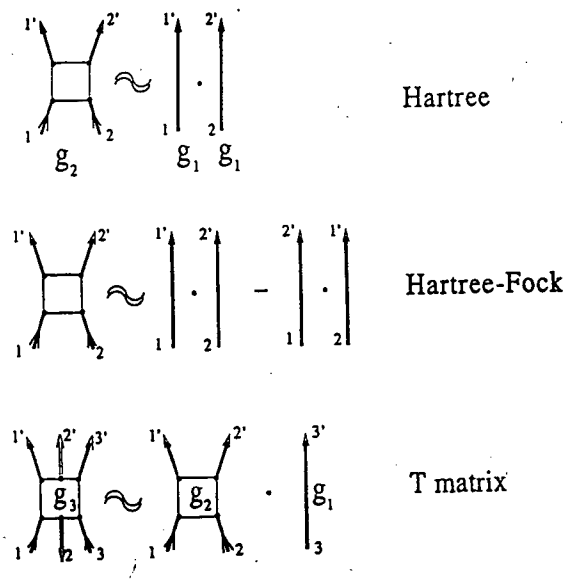

Figure 2: Factorization scheme of the four and six-point green's functions $g_2(12;1'2')$ and $g_3(123;1'2'3')$, respectively, which leads to the Hartee, Hartree-Fock (exchange term included), and T matrix approximations.

treatment of the many-body problem is achieved. The "Born" approximation of T sums the various meson potentials of the nucleon-nucleon interaction in free space, i.e.,

$$< 12 \mid v \mid 1'2' > = \sum_{M=\sigma,\omega,\pi,\varrho,\eta,\delta,\phi} \delta^4_{11'}\ \delta^4_{22'}\ \Gamma^M_{11'}\ \Gamma^M_{22'}\ \Delta^M_{12}\ , \tag{7}$$

and thus neglects dynamical nucleon-nucleon correlations. It is this approximation which leads to the Hartree and Hartree-Fock approximations [10, 23, 24, 25]. The symbol Γ in Eq. (7) stands for the various meson-nucleon vertices, and Δ^M denotes the free meson propagator of a meson of type M.

The nucleon self-energy (effective one-particle potential) is obtained from the T matrix by [10]

$$\Sigma^\Lambda \ = \ i \int [\ \mathrm{tr}\,(T\,g) - T\,g\ ]\,, \qquad \text{(ladder approximation)}\ , \tag{8}$$

and

$$\Sigma^{B,\mathrm{HF}} \ = \sum_{M=\sigma,\omega\,\pi,\varrho} \ \sum_{B'=p,n,\Sigma^{\pm,0},\Lambda,\Xi^{0,-},\Delta^{++,+,0,-}} \int [\ \mathrm{tr}\,(\Delta^M\,g^{B'}) - \Delta^M\,g^{B'}\ ]\ ,$$
$$\text{(Hartree} - \text{Fock approximation)}\ . \tag{9}$$

Equation (9) indicates that on the Hartree-Fock level the baryon self-energies include *all charged baryon states* whose threshold densities are reached in star models contructed from them. The nuclear forces in Eq. (9) are those of the scalar-vector-isovector model [28]. The baryon propagators in Eqs. (8) and (9) are given as the solutions of Dyson's equation,

$$g^B \ = \ g^{0B} \ + \ g^{0B}\,\Sigma^B(\{g^{B'}\})\,g^B\ , \tag{10}$$

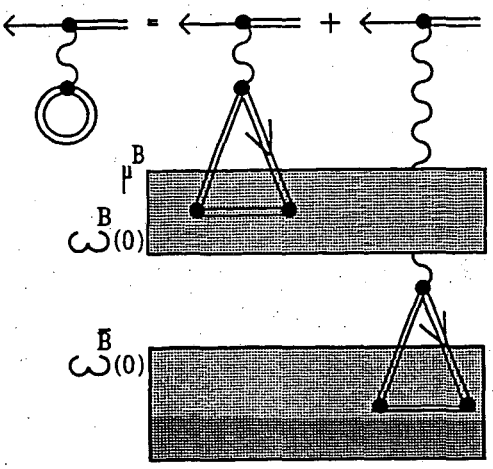

Figure 3: Graphical representation of the self-energy contributions (second term in Eq. (10)) arising from both the Fermi sea, i.e. nuclear matter consisting of filled baryon states of energies $\omega^B(0) \leq \omega^B(p) \leq \mu^B$ (upper graph), as well as Dirac sea (states $-\infty < \omega^{\bar{B}}(p) \leq \omega^{\bar{B}}(0)$, lower graph). The former (latter) lead to so-called medium (vacuum) polarization contributions [26, 27].

which terminates the set of equations that are to be solve self-consistently, subject to additional constraints of charge neutrality and generalized β-equilibrium [25, 29]. The diagrammatic representation of the second term in Dyson's equation, $g^{0B}\Sigma^B g^B$, is given in Fig. 3. There, single lines denote the free propagator, g^{0B}, and double lines refer to the self-consistent propagator in matter, g^B. This term corrects the free propagator functions (first term) for medium effects arising from the Fermi sea of filled baryon states, i.e. the nuclear matter medium (upper shaded area in Fig. 3), within which the baryons move.[1] Obviously these vanish for baryons propagating in free space, for which $\Sigma^B \equiv 0$. Note the mathematical structure of the matter equations: in order to calculate Σ^B, knowledge of the functions $g^{B'}$ ($B' = p, n, \Lambda$, etc., see Eq. (9)) is already necessary. Furthermore, in the framework of the ladder approximation, the T matrix possesses a functional dependence on the two-point function too. The determination of g^B from Dyson's equation thus leads to a self-consistent treatment of the coupled matter equations (6)-(10), and the functions g^B are referred to as self-consistent propagators.

The equation of state finally follows from the stress-energy density tensor $\mathcal{T}_{\mu\nu}$ of

[1] Contributions coming from the lower shaded area account for vacuum polarization corrections. The so-called no-sea approximation, which has been applied for the determination of most of the equations of state presented in Sec. 2.2, neglects such corrections. A critical discussion of the influence of vacuum renormalization on the equation of state of high-denity matter has been performed in Ref. [30]. It was found that these have negligible influence on the equation of state up to densities of at least ten times normal nuclear matter density, provided the coupling constants are tightly constrained by the saturation properties of nuclear matter. Here, vacuum polarization contributions are contained in equations of state denoted G_{300} and G^{π}_{300} (see Table 1) [30].

Table 1: Nuclear equations of state applied for the construction of models of general relativistic rotating neutron star models. Their tabulated representations, i.e. pressure versus energy and baryon density $P(\epsilon, \varrho)$, are given in Ref. [33]).

Label	EOS	Description (see text)	Reference
	Relativistic field theoretical equations of state		
1	G_{300}	H, K=300	[30]
2	HV	H, K=285	[29, 25]
3	G^{DCM2}_{B180}	Q, K=265, $B^{1/4}$ = 180	[4, 34]
4	G^{DCM2}_{265}	H, K=265	[35]
5	G^{π}_{300}	H, π, K=300	[30]
6	G^{π}_{200}	H, π, K=200	[36]
7	Λ^{00}_{Bonn} + HV	H, K=186	[8]
8	G^{DCM1}_{225}	H, K=225	[35]
9	G^{DCM1}_{B180}	Q, K=225, $B^{1/4}$ = 180	[4, 34]
10	HFV	H, Δ, K=376	[25]
11	Λ^{00}_{HEA} + HFV	H, Δ, K=115	[8]
	Non-relativistic potential model equations of state		
12	BJ(I)	H, Δ	[31]
13	WFF(UV_{14}+TNI)	NP, K=261	[17]
14	FP(V_{14}+TNI)	N, K=240	[37]
15	WFF(UV_{14}+UVII)	NP, K=202	[17]
16	WFF(AV_{14}+UVII)	NP, K=209	[17]

the system,

$$E(\varrho) = < \mathcal{T}_{00} > /\varrho - m \ , \qquad \text{with} \tag{11}$$

$$\mathcal{T}_{\mu\nu}(x) = \sum_{\chi=B,\lambda} \partial_\nu \Psi_\chi(x) \frac{\partial \mathcal{L}(x)}{\partial \left(\partial^\mu \Psi_\chi(x)\right)} - g_{\mu\nu}\, \mathcal{L}(x) \ . \tag{12}$$

The sum in the latter equation sums the contributions coming from the baryons and leptons ($\lambda = e, \mu$). The quantity $\mathcal{L}$ denotes the Lagrangian of many-baryon/lepton matter (see Ref. [25] for details).

2.2 Models for the nuclear equation of state

A representative collection of nuclear equations of state that are determined in the framework of non-relativisitic Schroedinger theory and relativistic nuclear field theory is listed in Table 1. A few of them are graphically shown in Fig. 4, where the pressure is plotted as a function of energy density (in units of the density of normal nuclear matter, ϵ_0 = 140 MeV/fm^3). This collection of equations of state has been applied for the construction of models of general relativistic rotating compact star models, which will be presented in Sec. 4.2. The specific properties of these equations of state are described in the third column of Table 1, where the following abbreviations

are used: N = pure neutron; NP = n, p, leptons; π = pion condensation; H = composed of n, p, hyperons ($\Sigma^{\pm,0}$, Λ, $\Xi^{0,-}$), and leptons; Δ = Δ_{1232}-resonance; Q = quark hybrid composition, i.e. n, p, hyperons in equilibrium with u, d, s-quarks, leptons; K = incompressibility (in MeV); $B^{1/4}$ = bag constant (in MeV). Not all equations of state of our collection account for neutron matter in β-equilibrium (i.e. entries 13-16). These models treat neutron star matter as being composed of only neutrons (entry 14), or neutrons and protons in equilibrium with leptons (entries 13, 15, 16), which is however not the ground-state of neutron star matter predicted by theory [29, 31, 32]. As an example of such an equation of state, we exhibit the FP(V_{14} + TNI) model in Fig. 4. The relativistic equations of state account for all baryon states that become populated in dense star models constructed from them. As representative examples for the relativistic equations of state, we show the HV, HFV, G_{300}, and G_{B180}^{DCM1} models in Fig. 4. A special feature of the latter equation of state is that it also (as G_{B180}^{DCM2}, which is not shown in Fig. 4) accounts for the possible transition of baryon matter to quark matter. One clearly sees in Fig. 4 the *softening of the equation of state*, i.e. reduction of pressure for a given density, at $\epsilon \gtrsim (2-3)\,\epsilon_0$ which is caused by the onset of baryon population and/or the transition of baryon matter to quark matter. The stiffer behavior of HFV in comparison with HV at high densities has its origin in the exchange (Fock) contribution that is contained in the former equation of state. An inherent feature of the relativistic equations of state is that they do not violate *causality*, i.e. the velocity of sound is smaller than the velocity of light at all densities, which is not the case for the non-relativistic models for the equation of state (cf. eighth column of Table 2). Among the latter only the WFF(UV_{14}+TNI) equation of state does not violate causality up to densities relevant for the construction of models of neutron stars from it.

The nuclear matter properties at saturation related to our collection of equations of state are summarized in Table 2. The listed quantities are: binding energy of normal nuclear matter at saturation density, $E(\varrho_0)/A$; compression modulus, $K(\varrho_0)$; effective nucleon mass, $M^*(\varrho_0)$ ($\equiv m^*(\varrho_0)/m$, where m denotes the nucleon mass); symmetry energy, $a_{sy}(\varrho_0)$. With the exception of Λ_{Bonn}^{00} + HV and Λ_{HEA}^{00} + HFV, the coupling constants of the relativistic equations of state are determined such that these saturate infinite nuclear matter at densities in the range $(0.15-0.16)$ fm^{-3} for a binding energy per nucleon of ≈ -16 MeV. For the Λ_{Bonn}^{00} + HV and Λ_{HEA}^{00} + HFV equations of state the saturation properties are determined by respectively the relativistic Bonn and HEA meson-exchange models for the nucleon-nucleon interaction whose parameters are determined by the free nucleon-nucleon scattering problem and the properties of the deuteron (parameter-free treatment). The influence of dynamical two-particle correlations calculated from the scattering matrix leads for these two equations of state to a relatively soft behavior in the vicinity of the saturation density ϱ_0. This is indicated by the rather small compression moduli K (and large effective nucleon masses) related to these equations of state. All non-relativistic equations of state of our collection, which are determined in the framework of the variational method outlined in Sec. 2.1.1, contain the impact of dynamical two-particle correlations in matter, too. The correlations are calculated for different Hamiltonians. With the exception of the BJ(I) model, the calculations are performed for the Urbana and Argonne two-nucleon potentials v_{14}, UV_{14} [38] and AV_{14} [39], respectively,

Table 2: Nuclear matter properties of the equations of state used in this work.

Label	EOS	E/A [MeV]	ϱ_0 [fm^{-3}]	K [MeV]	M^* [MeV]	a_{sy} [MeV]	ϵ/ϵ_0 †	Ref.
1	G_{300}	−16.3	0.153	300	0.78	32.5	–	[30]
2	HV	−15.98	0.145	285	0.77	36.8	–	[29, 25]
3	G^{DCM2}_{B180}	−16.0	0.16	265	0.796	32.5	–	[35]
4	G^{DCM2}_{265}	−16.0	0.16	265	0.796	32.5	–	[35]
5	G^{π}_{300}	−16.3	0.153	300	0.78	32.5	–	[30]
6	G^{π}_{200}	−15.95	0.145	200	0.8	36.8	–	[36]
7	Λ^{00}_{Bonn} + HV ‡	−11.9	0.134	186	0.79		–	[8]
8	G^{DCM1}_{225}	−16.0	0.16	225	0.796	32.5	–	[35]
9	G^{DCM1}_{B180}	−16.0	0.16	225	0.796	32.5	–	[35]
10	HFV	−15.54	0.159	376	0.62	30	–	[25]
11	Λ^{00}_{HEA} + HFV §	−8.7	0.132	115	0.82		–	[8]
12	BJ(I)						23.1	[31]
13	WFF(UV_{14}+TNI)	−16.6	0.157	261	0.65	30.8	> 14	[17]
14	FP(V_{14}+TNI)	−16.00	0.159	240	0.64		5.6	[37]
15	WFF(UV_{14}+UVII)	−11.5	0.175	202	0.79	29.3	6.5	[17]
16	WFF(AV_{14}+UVII)	−12.4	0.194	209	0.66	27.6	7.2	[17]

† Energy density in units of normal nuclear matter density beyond which the velocity of sound in neutron matter becomes larger (superluminal) than the velocity of light. The symbol "–" indicates that causality is not violated. As concerns WFF(UV_{14} + TNI), see text.

‡ T matrix calculation. The Bonn meson-exchange potential served as an input.

§ T matrix calculation. The HEA meson-exchange potential served as an input.

supplemented by different models for the three-nucleon interaction. These are the density-dependent three-nucleon interaction of Lagaris and Pandharipande, TNI [40], and the Urbana three-nucleon model, UVII [38] (see entries 13-16 in Table 2). One sees that nuclear matter is underbound by ≈ 4 MeV for two of these equations of state. The corresponding saturation densities ϱ_0 are in the range $(0.17 - 0.19)$ fm^{-3}, thus nuclear matter saturates at slightly too large densities for these equations of state. (The empirical saturation density is ≈ 0.15 fm^{-3} [41].) Equations of state labeled 13 and 14 lead to binding energies and saturation densities that are in good agreement with the empirical values which has its origin in the *density-dependent* three-nucleon interaction TNI.[2] A comparison with the relativistic parameter-free equations of state,

[2]It is well known that two-particle correlations alone fail in reproducing the empirical values of binding energy and saturation denstiy. In this case the saturation points calculated from the standard Brueckner-Hartree-Fock [14, 42, 43] and non-relativistic T matrix approximations [44, 45, 46] for different nucleon-nucleon interactions fall in a narrow band, often called the Coester band; it appears likely that this band would contain the calculated saturation point for *any realistic* nucleon-nucleon

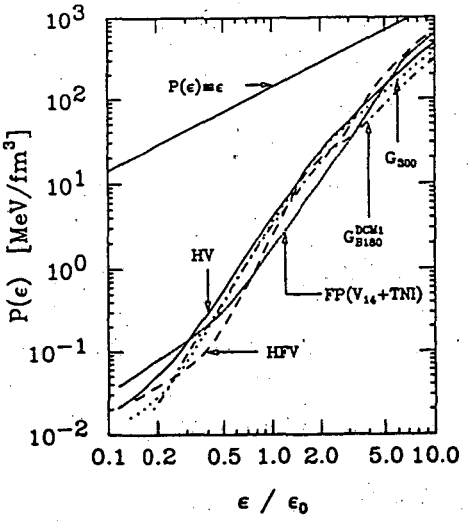

Figure 4: Graphical illustration of the equations of state HV, HFV, FP(V_{14} + TNI), G_{300}, and G^{DCM1}_{B180}.

Λ^{00}_{Bonn} + HV and Λ^{00}_{HEA} + HFV, shows that these saturate nuclear matter at somewhat smaller densities in the range $(0.13 - 0.16)$ fm^{-3}. The corresponding binding energies lie respectively ≈ 4 and ≈ 7 MeV above the the epirical value, thus nuclear matter is considerably underbound for these models. Interesting is the shift of the saturation density relative to non-relativistic treatments toward smaller values which is caused by relativity [23, 26, 49, 50, 51]. For this reason the Λ^{00}_{Bonn} + HV and Λ^{00}_{HEA} + HFV equations of state saturate at $\varrho_0 = 0.13$ fm^{-3}, which is smaller than the above given range related to the non-relativistic potential models.

The four equations of state G^{DCM1}_{225}, G^{DCM2}_{265}, G^{DCM1}_{B180}, and G^{DCM2}_{B180}, which are based on the relativistic Lagrangian of Zimanyi and Moszkowski, have only recently been determined [34, 52]. The transition of confined hadronic matter into quark matter is taken into account in equations of state G^{DCM1}_{B180} (Fig. 4) and G^{DCM2}_{B180}. Here a bag constant of $B^{1/4} = 180$ MeV has been used for the determination of the transition of baryon matter into quark matter, which places the energy per baryon of strange matter at 1100 MeV, well above the energy per nucleon in ^{56}Fe (≈ 930 MeV). Most interestingly, the transition to quark matter sets in already at a density $\epsilon = 2.3\,\epsilon_0$ [4, 34], which lowers the pressure relative to confined hadronic matter. The mixed phase of baryons and quarks ends, i.e. the pure quark phase begins, at $\epsilon \approx 15\,\epsilon_0$, which is larger than the central density encountered in the maximum-mass star model constructed from this equation of state. We stress that these density thresholds are rather different from those computed by other authors in earlier investigations. The reason for this lies in the realization that the transition between confined hadronic matter and quark matter takes place subject to the conservation of baryon and electric charge. Correspondingly, there are *two* chemical potentials, and the transition of baryon matter to quark matter is to be determined in three-space spanned by pressure and the chemical potentials of the electrons *and* neutrons. The only existing investi-

interaction [47, 48].

gation which accounts for this properly has been performed by Glendenning [4, 34]. (An investigation of the structure of the mixed phase of baryons and quarks has recently been performed by Heiselberg, Pethick, and Staubo [53].) Further important differences between the determination of G_{B180}^{DCM1} and earlier (and thus inconsistent) treatments concern the description of the dense interior of compact stars[3] and the approximation of the mixed phase as two components which are separately charge neutral.

3 Observed neutron star properties

The global neutron star properties such as masses, rotational frequencies, radii, moments of inertia, redshifts, etc. are known to be sensitive to the adopted microscopic model for the nucleon-nucleon interaction or, in other words, to the nuclear equation of state [63]. Thus, by means of comparing the theoretically determined values for these quantities with observed ones one may hope to learn about the physical behavior of matter at super-nuclear densities. In the following we briefly summarize important star properties.

3.1 Masses

The gravitational mass is of special importance since it can be inferred directly from observations of X-ray binaries and binary pulsars (e.g. the Hulse-Taylor radio pulsar PSR 1913+16 [64]). Rappaport and Joss were the first who deduced neutron star masses for six X-ray binaries [65]. A reexamination of these masses became possible owing to the improved determinations of orbital parameters [66]. The improved values are

$$1.56 \leq M\,(\text{4U 0900}-40)/M_\odot \leq 1.98\,, \qquad 0.96 \leq M\,(\text{4U 1538}-52)/M_\odot \leq 2.75\,,$$

$$0.75 \leq M\,(\text{SMC X}-1)/M_\odot \leq 1.39\,, \qquad 0.53 \leq M\,(\text{Cen X}-3)/M_\odot \leq 1.62\,,$$

$$0.88 \leq M\,(\text{LMC X}-4)/M_\odot \leq 1.88\,, \qquad 0.86 \leq M\,(\text{Her X}-1)/M_\odot \leq 1.1\,,$$

and the most probable masses are

$$M\,(\text{4U 0900}-40)/M_\odot = 1.77\,, \qquad M\,(\text{4U 1538}-52)/M_\odot = 1.79\,,$$

$$M\,(\text{SMC X}-1)/M_\odot = 1.06\,, \qquad M\,(\text{Cen X}-3)/M_\odot = 1.06\,,$$

$$M\,(\text{LMC X}-4)/M_\odot = 1.38\,, \qquad M\,(\text{Her X}-1)/M_\odot = 0.98\,.$$

[3] If the dense core may be converted to quark matter [54, 55, 56], it must be ***strange quark matter***, since 3-flavor quark matter has lower energy than 2-flavor and just as is the case for the hyperon content of neutron stars, strangeness is not conserved on macroscopic time scales. Many of the earlier discussions [54, 55, 56, 57, 58, 59, 60, 61, 62] have treated the neutron star as pure in neutrons, and the quark phase as consisting of the equivalent number of u and d quarks. However neither is pure neutron matter the ground state of a star nor is a mixture of $n_d = 2\,n_u$! In fact it is a highly excited state, and will quickly weak decay to an approximate equal mixture of u, d, s quarks.

Estimates of the limits of the masses of two non-pulsating X-ray binaries are (it is expected that at least one of these objects, likely Cyg X-1, is a black hole):

$$M\,(3\mathrm{U}\ 1700-37)/M_\odot \geq 0.6\,, \qquad 0.9 \leq M\,(\mathrm{Cyg\,X}-1)/M_\odot \leq 15\,.$$

Finally we note the extremely accurately determined mass of the Hulse-Taylor binary pulsar PSR 1913+16 which is given by [64]

$$M(\mathrm{PSR}\ 1913+16)/M_\odot = 1.444 \pm 0.003\,.$$

In summary, neutron star mass determinations derived from observations of binary X-ray pulsars suggest that the most probable values of neutron star mass is close to $1.4\,M_\odot$, but the masses of individual neutron stars are likely to be in the range $1.1 \lesssim M/M_\odot \lesssim 1.8$ [66].

3.2 Rotational frequencies of fast pulsars

The rotational periods of fast pulsars provide conditions on the equation of state when combined with the mass constraint [67]. As already mentioned in Sec. 1, the fastest so far observed pulsars have rotational periods of 1.6 ms (see Fig. 1). The successful model for the nuclear equation of state, therefore, must account for rotational neutron star periods of at least $P = 1.6$ ms as well as masses that lie in range listed in Sec. 3.1.

3.3 Radii

Direct radius determinations for neutron stars do not exist. However, combinations of data of 10 well-observed X-ray bursters with special theoretical assumptions lead Van Paradijs [68] to the conclusion that the emitting surface has a radius of about 8.5 km. This value, as pointed out in [69], may be underestimated by a factor of two. Fujimoto and Taam [70] derived from the observational data of the X-ray burst source MXB $1636-536$, under rather uncertain theoretical assumptions, a neutron star mass and radius of $1.45\,M_\odot$ and 10.3 km. An error analysis lead them to predicting mass and radius ranges of 1.28 to $1.65\,M_\odot$ and 9.1 to 11.3 km, respectively. When comparing these values with computed neutron star data, however, one should be aware of the fact that burster are suspected, but not known, to be neutron stars.

3.4 Moment of inertia

Another global neutron star property is the moment of inertia, I. Early estimates of the energy-loss rate from pulsars [71] spanned a wide range of I: $7 \times 10^{43} < I < 7 \times 10^{44}$ g/cm^3. From the luminosity of the Crab nebula ($\sim 2-4 \times 10^{38}$ erg/sec), several authors have found a lower bound on the moment of inertia of the pulsar given by $I \gtrsim 4-8 \times 10^{44}$ g cm^2 [72, 73, 74].

3.5 Redshift

Finally we mention the neutron star redshift, z. Liang [75] has considered the neutron star redshift data base provided by measurements of γ-ray burst redshifted annihilation lines in the range $300 - 511$ keV. These bursts have widely been interpreted as gravitationally redshifted 511 keV $e^{\pm}$ pair annihilation lines from the surfaces of neutron stars. From this he showed that there is tentative evidence (if the interpretation is correct) to support a neutron star redshift range of $0.2 \leq z \leq 0.5$, with the highest concentration in the narrower range $0.25 \leq z \leq 0.35$. A particular role plays the source of the 1979 March 5 γ-ray burst source, which has been identified with SNR N49 by its position. From the interpretation of its emmision, which has a peak at ~ 430 keV, as the 511 keV $e^{\pm}$ annihilation line [76, 77] the resulting gravitational redshift has a value of $z = 0.23 \pm 0.05$.

3.6 Glitches

Glitches are sudden relatively small changes in the period of pulsars, which otherwise increase very slowly with time due to the loss of rotational energy through radiation. They occur in various pulsars at intervals of days to months or years, and in some pulsars are small (Crab), and in others large (Vela) and infrequent ($\Delta\Omega/\Omega \sim 10^{-8} - 10^{-6}$ respectively). If the star quake model for glitches is correct [78, 79], the characteristic time between two glitches, or quakes, (the so-called interglitch time) is given by

$$t_q \;=\; 3.553 \times 10^6 \, \frac{[(M_P \,-\, M)/M_\odot]^2}{R_5^3 \, I_{45}} \quad \text{yr} \;. \tag{13}$$

Here R_5 is the radius in kilometers, I_{45} the moment of inertia in units of 10^{45} g cm^2, and M_P and M denote the proper respectively gravitational mass [80]. The interglitch time is given in years. Furthermore we note that in order to arrive at Eq. (13) an iron crust ($Z = 26$) has been assumed, and for Ω and $d\Omega/dt$ the observational data from the Crab pulsar ($T \approx 2260$ yr) and an oblateness change of $\Delta\epsilon \approx 0.9 \times 10^{-9}$ has been taken.

4 Properties of compact star

4.1 Non-rotating star models

Figure 5 exhibits the spherical neutron star mass, in units of the solar mass, as a function of central energy density for a sample of equations of state of Table 1. The star sequences are shown up to densities that are slightly larger than those of the maximum-mass stars (indicated by tick marks). One sees that all equations of state are able to support non-rotating neutron star models of gravitational masses $M \geq M(\text{PSR } 1913 + 16)$. On the other hand, rather massive stars of say $M \gtrsim 2\,M_\odot$ can only be obtained for a few equations of state, depending on their stiffness at large nuclear densities (cf. Fig. 4). The largest maximum-mass, $M = 2.2\,M_\odot$, is obtained for HFV. Knowledge of the maximum-mass value is of importance for two reasons. Firstly, quite a few neutron star masses are known (Sec. 3), and the largest of these

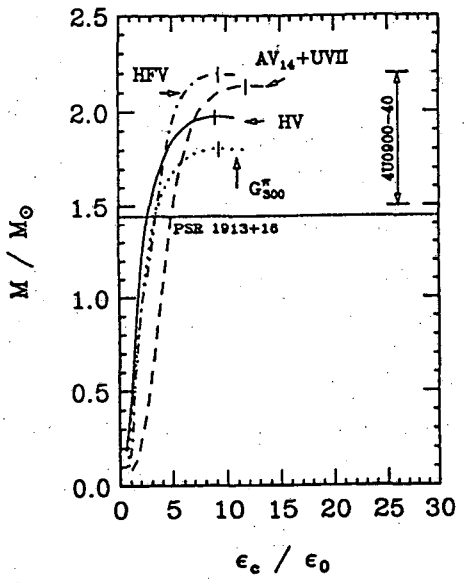

Figure 5: Non-rotating neutron star mass as a function of central density.

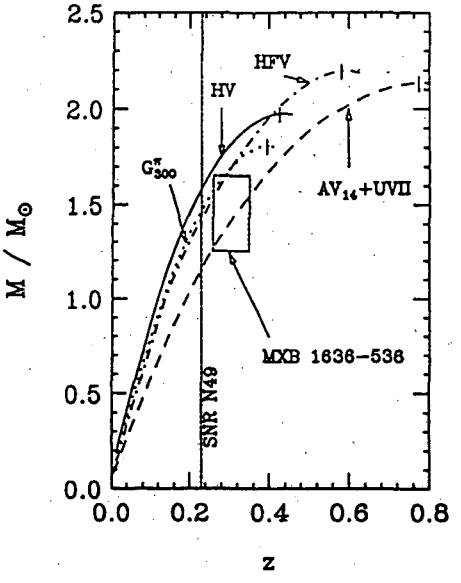

Figure 6: Non-rotating neutron star mass as a function of redshift.

imposes a lower bound on the maximum-mass of a theoretical model. The current lower bound is $1.56\,M_\odot$ (neutron star 4U 0900 − 40), which, as we have just seen, does not set a too stringent constraint on the nuclear equation of state. The situation could easily change if an accurate future determination of the mass of neutron star 4U 0900 − 40 (see Fig. 5) should result in a value that is close to its present upper bound of $1.98\,M_\odot$. In this case most of the equations of state of our collection would be ruled out! (Only entries 10,11,15, and 16 in Table 1 can easily account for such a heavy neutron star [33].) The second reason is that the maximum mass can be useful in identifying black hole candidates [81]. For example, if the mass of a compact companion of an optical star is determined to exceed the maximum mass of a neutron star it must be a black hole. Since the maximum mass of stable neutron stars in our theory is $2.2\,M_\odot$, compact companions being more massive than that value are predicted to be black holes.

The neutron star mass as a function of gravitational redshift is displayed in Fig. 6 for the same sample of equations of state as in Fig. 5. One sees that the maximum-mass stars can have redshifts in the range $0.4 \lesssim z \lesssim 0.8$, depending on the equation of state. Neutron stars of typically $M \approx 1.5\,M_\odot$ (e.g. PSR 1913+16) are predicted to have redshifts in the considerably narrower range $0.2 \leq z \leq 0.32$. The solid rectangle covers masses and redshifts in the ranges of respectively $1.30 \leq M_s/M_\odot \leq 1.65$ and $0.25 \leq z \leq 0.35$. As outlined in Secs. 3.3 and 3.5, the former range has been determined from observational data of X-ray burst source MXB 1636 − 536 [70], while the latter is based on the neutron star redshift data base provided by measurements of gamma-ray burst pair annihilation lines [75] (note however the critical remarks in Secs. 3.3 and 3.5 concerning the interpretation of these data). From the redshift value of SNR N49 (if correct) we predict a neutron mass star of $1.1 \lesssim M/M_\odot \lesssim 1.6$, which is consitent with the observed mass range given in Sec. 3.1. The relativistic equations of state set a narrower mass limit for SNR N49, $1.4 \lesssim M/M_\odot \lesssim 1.6$.

Figure 7 displays the radius as a function of gravitational redshift. The solid

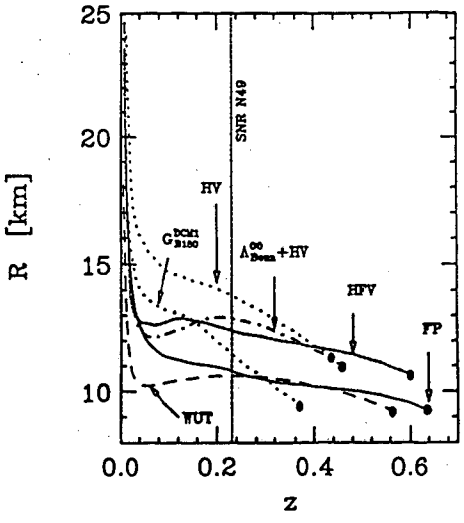

Figure 7: Radius as a function of redshift for a sample of equations of state of Table 1.

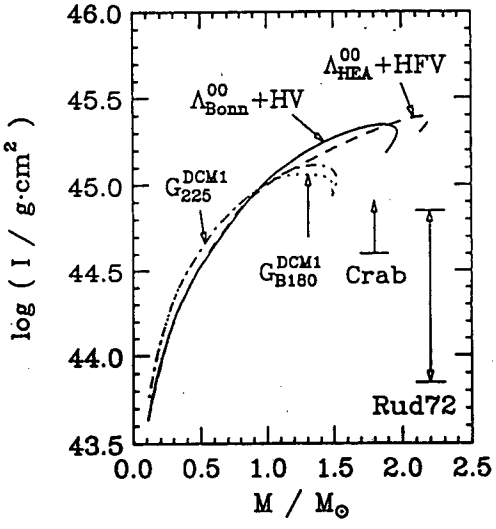

Figure 8: Moment of inertia as a function of mass for a sample of equations of state of Table 1.

dots refer to the maximum-mass star of each sequence. Of course, stars at their termination points possess the largest redsifts, and these become the smaller the lighter the stars. Under the assumption that the annihilation line interpretation is correct (Sec. 3.5), SNR N49 is predicted to have a radius in the range of $10 - 14$ km, which is consistent with the rather broad range given in Sec. 3.3. The relativistic equations of state lead to a narrower radii range, $12.5 - 14$ km. In general, the non-relativistic equations of state lead to smaller radii for a given redshift. The reason for this lies in the relatively soft (stiff) behavior at low (high) nuclear densities of the non-relativistic equations of state, which is less pronounced for the relativistic equations of state. Small radius values of star models are important in order to achieve rapid rotation. For that reason star models constructed for the non-relativistic equations of state possess limiting rotational periods that are smaller than those obtained for the relativistic equations of state(Sec. 4.2). However, because of causality violation of the non-relativistic equations of state at high nuclear densities (Sec. 2.2), this trend may be considered as an artifact.

In Fig. 8 we show the moment of inertia as a function of mass. In Sec. 2.2 we have pointed out that, in general, the inclusion of baryon population in neutron star matter as well as the possible transition of confined hadronic matter to quark matter causes a softening of the equation of state which leads to somewhat smaller star masses and radii. Since $I \propto R_s^2 M_s$ one expects a relative decrease of the moment of inertia of star models constructed for such equation of state.[4] By means of comparing the curves labeled G_{B180}^{DCM1} and G_{225}^{DCM1} with each other one sees the impact of the transition into quark matter on I. The difference however is rather small, as is the case for other star

[4]Of course, the general relativistic expression for the moment of inertia is more complicated. It accounts for the dragging effect of inertial frames and the curvature of space [82]. The qualitative dependence of the moment of inertia on mass and radius as expressed in the classical expression for the moment of inertia remains valid [63].

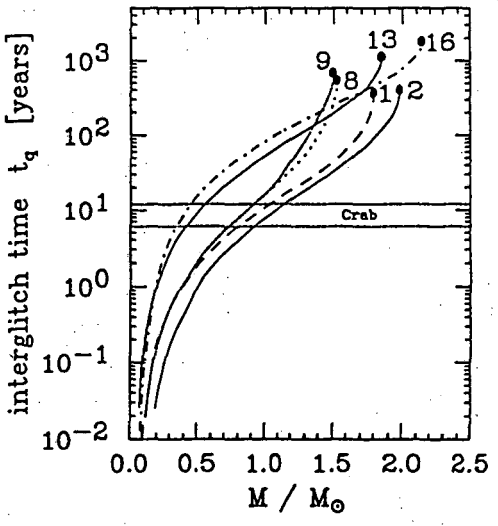

Figure 9: Interglitch time between two successive pulsar glitches as a function of star mass.

properties. Therefore one cannot expect that the transition might register itself in observational quantities. (This is different, to some extent, for a hypothetical strange stars which will be discussed in Sec. 5). Estimates for the upper and lower bounds on the moment of inertia of the Crab pulsar derived from the pulsar's energy loss rate (labeled Rud72), and the lower bound on the moment of inertia derived from the luminosity of the Crab nebula (labeled Crab) [72, 73, 74] are shown in Fig. 8 for the purpose of comparison. (The arrows refer only to the value of $I_{\rm Crab}$ and not to its mass, which is not known.)

The interglitch time, calculated from Eq. (13), as a function of star mass is plotted in Fig. 9 for a few representative equations of state. It is striking that t_q depends rather sensitively on M. For example, considering $t_q \sim 10$ yr as compatible with observational evidence for glitches, we obtain masses in the range $\approx 0.3 - 1.1\, M_\odot$. Conversely, if we assume values of $M \approx 1.4 - 1.5\, M_\odot$ as the most probable Crab pulsar mass, the interglitch time ranges from 30 to 700 years! In the case that the Crab pulsar would be a medium massive neutron star of say $M \approx 1\, M_\odot$, the interglitch times obtained for the relativistic equations of state are compatible with observation, provided, of course, the star quake model for glitches is correct. In order to obtain compatibility with star models constructed for the non-relativistic equations of state, the pulsar's mass must be $M \approx 0.4\, M_\odot$.

4.2 Rotating star models

4.2.1 Minimum rotational period set by the gravitational radiaion-reaction instability

Figures 10 and 11 exhibit the limiting rotational periods of compact stars, which is set by the gravitational radiation reaction-driven instability [83, 84, 85]. Figure 10 refers to hot ($T = 10^{10}$ K), newly born stars in supernova explosions (i.e., pulsars). Figure 11 is the analog of Fig. 10, but for old and therefore cold compact stars of temperature

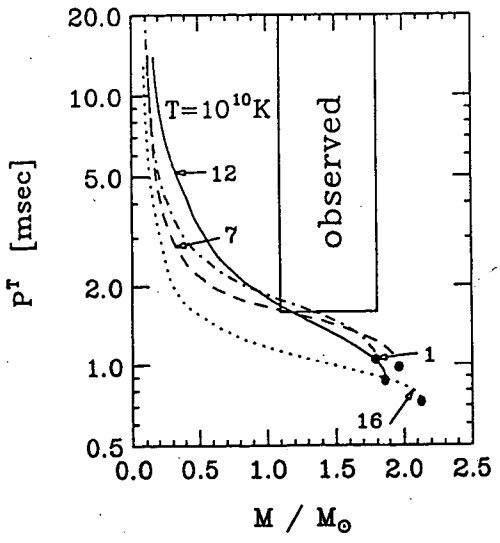

Figure 10: Gravitational radiation instability period P^T versus mass for newly born stars of temperature $T = 10^{10}$ K [89].

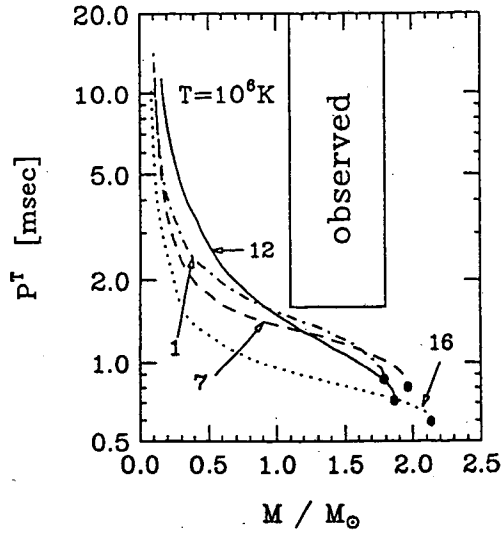

Figure 11: Gravitational radiation instability period P^T versus mass for old stars of temperature $T = 10^6$ K [89].

$T = 10^6$ K, like neutron stars in binary systems that are being spun up (and thereby reheated) by mass accretion from a companion. One sees that the limiting periods P^T ($\equiv 2\pi/\Omega^T$, where Ω^T denotes the temperature dependent rotational star frequency) are the smaller the more massive (and thus the smaller the radius) the star model (cf. Fig. 7). A comparison between Figs. 10 and 11 shows that the instability periods are shifted toward smaller values the colder the star. Consequently, the instability modes of compact stars in binary systems are excited at smaller rotational periods than is the case for hot and newly born pulsars in supernovae.[5] The dependence of P^T on the equation of state is shown too in these figures. One sees that the lower limits on P^T are set by the non-relativistic equation of state labeled 16 due to the small radii values obtained for the star models constructed from it. The relativistic models for the equation of state generally lead to larger rotational periods due to the somewhat larger radii of the associted star models.

The rectangles in Figs. 10 and 11 denoted "observed" cover both observed star masses, $1.1 \leq M/M_\odot \leq 1.8$, and observed pulsar periods, i.e. $P \geq 1.6$ ms (see Fig. 1). One sees that even the most rapidly rotating pulsars so far observed can be understood as rotating neutron or hybrid stars.[6] The observation of pulsars possessing masses in

[5]Sawyer [86] has found that the *bulk* viscosity of neutron star matter goes as the sixth power of the temperature, as compared with a T^{-2} dependence for the *shear* viscosity which is treated here. This means that at $T \gtrsim 10^9$ K the bulk viscosity would dominate over the shear viscosity and thus damp the gravitational-wave instability. In this case the instability periods would be shifted toward values that are relatively close to the Kepler period P_K [87, 88], which sets an *absolute* limit on stable rotation because of mass shedding. Bound for the P_K are given in Table 3.

[6]Depending on their composition, compact star models are denoted as neutron, hybrid, or strange stars. Neutron stars consist of protons, neutrons and more massive baryons in β-equilibrium with leptons; hybrid stars are compact stars which, in addition to baryons, also contain quarks in their dense cores; hypothetical strange stars consist of (3-flavor) strange-quark-matter which, by hypoth-

the observed range but rotational periods that are smaller than say $\sim$ 1 ms (depending on temperature and thus on the pulsar's history) would be in clear contradiction to our equations of state. Consequently the observation of such pulsars cannot be reconciled with the interpretation of such objects as rapidly rotating *neutron or hybrid* stars. An investigation of the limiting rotational Kepler period of neutron and other compact stars that is performed *without* taking recourse to any particular models of dense matter (but derives the limit only on the general principles that: Einstein's equations describe stellar structure, matter is microscopically stable, and causality is not violated) has only recently been performed by Glendenning [90]. He establishes a lower bound for the minimum Kepler period for a $M = 1.442\,M_\odot$ neutron star of $P_K = 0.33$ ms. Of course the equation of state that nature has chosen need not be the one that allows stars to rotate most rapidly. On the basis of the neutron star models constructed from the selection of equations of state studied here, the lowest Kepler period was found to be 0.7 ms (cf. Table 3).

4.2.2 Bounds of fast pulsars

Here we restrict ourselves to discussing the properties of a rapidly rotating pulsar model having a mass of $M \approx 1.45\,M_\odot$, as supported by the evolutionary history of supermassive stars [69]. The bounds on its properties, whose knowlege is of great importance for the interpretation of fast pulsar, are summarized in Table 3. The listed properties are: period at which the gravitational radiation-reaction instability sets in, P^T (in ms) with star temperature listed in parentheses; Kepler period, P_K (in ms); central density, ϵ_c (in units of the density of normal nuclear matter); moment of inertia, I (in g cm^2); redshifts of photons emitted at the star's equator in backward (z_B) and forward (z_F) direction. According to Table 3, newly born pulsars observed in supernova explosions can only rotate stably at periods $\gtrsim$ 1 ms. Half-millisecond periods, for example, are completely excluded for pulsars made of baryon matter. Therefore, the possible future discovery of a single sub-millisecond pulsar, rotating with a period of say $\sim$ 0.5 ms, would give a strong hint that such an object is a rotating *strange star*, not a neutron star, and that 3-flavor strange quark matter is the true ground-state of the strong interaction, as pointed out by Glendenning [91]. An old pulsar of $T = 10^6$ K (and mass $M \approx 1.45\,M_\odot$) cannot be spun up to stable rotational periods smaller than $\approx$ 0.8 ms. Again, the two fastest yet observed pulsars, rotating at 1.6 ms, are compatible with the periods in Table 3, provided their masses are larger than 1 $M_\odot$ [89]. For the purpose of comparison the Kepler period, below which mass shedding at the star's equator sets in, is listed too. It might play a role in cold (hot) pulsar whose rotation is stabilized by its large shear (bulk) viscosity value (see footnote on Sawyers calculation of the viscosity in dense nuclear matter).

esis, forms the absolute ground-state of the strong interaction (see Sec. 5 for more details).

Table 3: For the broad sample of equations of state, the lower and upper bounds on the properties of a pulsar of $M \approx 1.45\,M_\odot$, calculated for the collection of equations of state of Table 1 [92].

	$P(10^6\ K)$	$P(10^{10}\ K)$	P_K	ϵ_c/ϵ_0	$\log I$	z_B	z_F	z_p
upper bound	1.1	1.5	1	5	45.19	1.05	−0.18	0.45
lower bound	0.8	1.1	0.7	2	44.95	0.59	−0.21	0.23

5 Strange stars

5.1 The strange matter hypothesis

The hypothesis that strange quark matter may be the absolute ground state of the strong interaction (not ^{56}Fe) has been raised by Witten in 1984 [11]. If the hypothesis is true, then a *separate* class of compact stars could exist, which are called strange stars. They form a distinct and disconnected branch of compact stars and are not part of the continuum of equilibrium configurations that include white dwarfs and neutron stars. In principle both strange and neutron stars could exist. However if strange stars exist, the galaxy is likely to be contaminated by strange quark nuggets which would convert all neutron stars that they come into contact with to strange stars [91, 93, 94]. This in turn means that the objects known to astronomers as pulsars are probably rotating strange matter stars, *not* neutron matter stars as is usually assumed. Unfortunately the bulk properties of models of neutron and strange stars of masses that are typical for neutron stars, $1.1 \lesssim M/M_\odot \lesssim 1.8$, are relatively similar and therefore do not allow the distiction between the two possible pictures. The situation changes however as regards the possibility of *fast rotation* of strange stars. This has its origin in the completely different mass-radius relations of neutron and strange stars (see Fig. 12) [54]. As a consequence of this the entire familiy of strange stars can rotate rapidly, not just those near the limit of gravitational collapse to a black hole as is the case for neutron stars. As an example, above the minimum possible rotational periods of maximum-mass neutron and hybrid stars have been determined to be larger than ≈ 0.8 ms; this is to be compared with $\approx (0.4 - 0.6)$ ms calculated for maximum-mass strange stars [82].

5.2 Hadronic crust on strange stars

At the present time there appears to be only one crucial *astrophysical test* of the strange-quark-matter hypothesis, and that is whether strange quark stars can give rise to the observed phenomena of pulsar glitches (see Sec. 3.6). In the crust quake model an oblate solid nuclear crust in its present shape slowly comes out of equilibrium with the forces acting on it as the rotational period changes, and fractures when the built up stress exceeds the sheer strength of the crust material. The period and rate of change of period slowly heal to the trend preceding the glitch as the coupling between

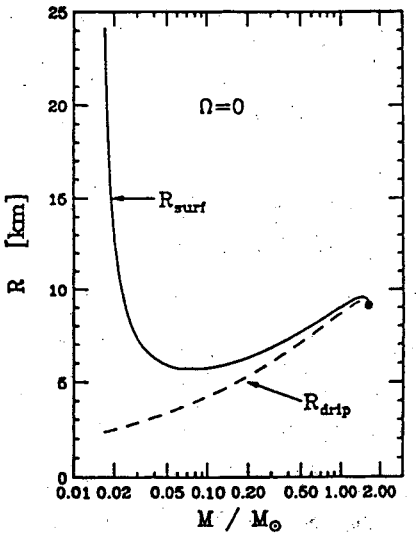

Figure 12: Radius as a function of mass of a non-rotating strange star with crust [82].

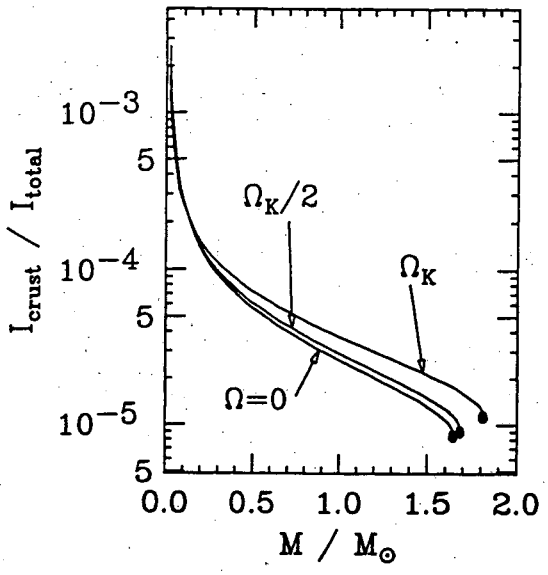

Figure 13: The ratio $I_{\rm crust}/I_{\rm total}$ as a function of star mass. Rotational frequencies are shown as a fraction of the Kepler frequency, $\Omega_{\rm K}$ [4].

crust and core re-establish their co-rotation. The existence of glitches may have a decisive impact on the question of whether strange matter is the ground state of the strong interaction.

The only existing investigation which deals with the calculation of the thickness, mass and moment of inertia of the nuclear solid crust that can exist on the surface of a rotating, general relativistic strange quark star has only recently been performed by Glendenning and Weber [82]. Their calculated mass-radius relationship for strange stars with a nuclear crust, whose maximum density is the neutron drip density, is shown in Fig. 12. (Free neutron in the star cannot exist. These would be dissolved into quark matter as they gravitate into the core. Therefore the maximum density of the crust is strictly limited by neutron drip. This density is about 4.3×10^{11} g/cm^3.) Since the crust is bound by the gravitational interaction (and not by confinement, which is the case for the strange matter core), the relationship is qualitatively similar to the one for neutron and hybrid stars, as can be seen from Fig. 7. The radius being largest for the lightest and smallest for the heaviest stars (indicated by the soid dot in Fig. 12) in the sequence. Just as for neutron stars the relationship is not necessarily monotonic at intermediate masses. The radius of the strange quark core, denoted $R_{\rm drip}$, is shown by the dashed line. (A value for the bag constant of $B^{1/4} = 160$ MeV for which 3-flavor strange matter is stable has been chosen. This choice represents weakly bound strange matter with an energy per baryon ~ 920 MeV, and thus corresponds to strange quark matter being absolutely bound with respect to ^{56}Fe). The radius of the strange quark core is proportional to $M^{1/3}$ which is typical for self-bound objects. This proportionality is only modified near the mass where gravity terminates the stable sequence. The sequence of stars has a minimum mass of $\sim 0.015\,M_\odot$ (radius of ~ 400 km) or about 15 Jupiter masses, which is smaller than that of neutron star sequences, about 0.1 $M_\odot$ [95]. The low-mass strange stars may

be of considerable importance since they may be difficult to detect and therefore may effectively *hide baryonic matter*. Furthermore, of interest to the subject of cooling of strange stars is the crust thickness of strange stars [96]. It ranges from $\sim$ 400 km for stars at the lower mass limit to $\sim$ 12 km for stars of mass $\sim 0.02\,M_\odot$, and is a fraction of a kilometer for the star at the maximum mass [82].

The moment of inertia of the hadronic crust, $I_{\rm crust}$, that can be carried by a strange star as a functin of star mass for a sample of rotational frequencies of $\Omega = \Omega_{\rm K}, \Omega_{\rm K}/2$ and 0 is shown in Fig. 13. Because of the relatively small crust mass of the maximum-mass models of each sequence, the ratio $I_{\rm crust}/I_{\rm total}$ is smallest for them (solid dots in Fig. 13). The less massive the strange star the larger its radius (Fig. 12) and therefore the larger both $I_{\rm crust}$ as well as $I_{\rm total}$. The dependence of $I_{\rm crust}$ and $I_{\rm total}$ on M is such that their ratio $I_{\rm crust}/I_{\rm total}$ is a monotonically decreasing function of M. One sees that there is only a slight difference between $I_{\rm crust}$ for $\Omega = 0$ and $\Omega = \Omega_{\rm K}/2$.

Of considerable relevance for the question of whether strange stars can exhibit glitches in rotation frequency, one sees that $I_{\rm crust}/I_{\rm total}$ varies between 10^{-3} and $\sim 10^{-5}$ at the maximum mass. If the angular momentum of the pulsar is conserved in the quake then the relative frequency change and moment of inertia change are equal, and one arrives at [82]

$$\frac{\Delta\Omega}{\Omega} = \frac{|\Delta I|}{I_0} > \frac{|\Delta I|}{I} \equiv f\,\frac{I_{\rm crust}}{I} \sim (10^{-5} - 10^{-3})\,f \ , \text{ with} \qquad 0 < f < 1 \ . \quad (14)$$

Here I_0 denotes the moment of inertia of that part of the star whose frequency is changed in the quake. It might be that of the crust only, or some fraction, or all of the star. The factor f in Eq. (14) represents the fraction of the crustal moment of inertia that is altered in the quake, i.e. $|\Delta I| = f\,I_{\rm crust}$. Since the observed glitches have relative frequency changes $\Delta\Omega/\Omega = (10^{-9} - 10^{-6})$, a change in the crustal moment of inertia by less than 10% would cause a giant glitch even in the least favorable case (for more details, see [82]). Finally we find that the observed range of the fractional change in $\dot\Omega$ is consistent with the crust having the small moment of inertia calculated and the quake involving only a small fraction f of that, just as in Eq. (14). For this purpose we write [82]

$$\frac{\Delta\dot\Omega}{\dot\Omega} = \frac{\Delta\dot\Omega/\dot\Omega}{\Delta\Omega/\Omega}\,\frac{|\Delta I|}{I_0} = \frac{\Delta\dot\Omega/\dot\Omega}{\Delta\Omega/\Omega}\,f\,\frac{I_{\rm crust}}{I_0} > (10^{-1}\ \text{to}\ 10)\,f \ , \quad (15)$$

which yields a small f value as before: $f < (10^{-4}$ to $10^{-1})$. Here measured values of the ratio $(\Delta\Omega/\Omega)/(\Delta\dot\Omega/\dot\Omega) \sim 10^{-6}$ to 10^{-4} for the Crab and Vela pulsars, respectively, have been used.

6 Summary

This work begins with an investigation of the properties of superdense nuclear matter. Various models for the associated equation of state are introduced and discussed in greater detail. These equations of state are then applied for the construction of models of non-rotating as well as rotating compact stars, whose properties are compared with observational data. Our particular interest is aimed toward answering the following questions:

- Can a compact star rotate rapidly and with a central density that is plausibly below the transition point at which matter consisting of individual nucleons will dissolve into quark matter so that it is a neutron star?
- Can a hybrid star, a neutron star with a quark core, rotate very rapidly?
- What is the minimum rotational period in either case?
- Can strange stars give rise to the observed phenomena of pulsar glitches?

The indication of this work is that the gravitational radiation-reaction instability sets a lower limit on stable rotation for massive *neutron or hybrid stars* of $P \approx 0.8$ ms. Lighter ones having typical pulsar masses of $1.45\,M_\odot$ are predicted to have rotational periods $P \gtrsim 1$ ms. This finding may have very important implications for the nature of any pulsar that is found to have a shorter period, say below $P \lesssim 0.5$ ms. Since our representative collection of nuclear equations of state does not allow for rotation at such small periods, the interpretation of such objects as rapidly rotating neutron or hybrid stars fails. Such objects, however, can be understood as rapidly rotating *strange stars*. The plausible ground-state state in that event is the deconfined phase of (3-flavor) strange-quark-matter. From the QCD energy scale this is as likely a ground-state as the confined phase. At the present time there appears to be only one crucial astrophysical test of the strange-quark-matter hypothesis, and that is whether strange quark stars can give rise to the observed phenomena of pulsar glitches. We demonstrate that the nuclear solid crust that can exist on the surface of a strange star can have a moment of inertia sufficiently large that a fractional change can account for the magnitude of pulsar glitches. Furthermore low-mass strange stars can have enormously large nuclear crusts (up to ~ 400 km) which might considerably alter the cooling rate of strange stars and enables such objects to be possible hiding places of baryonic matter.

If strange-quark-matter is the ground-state of baryonic matter at zero pressure then the conclusion that the confined hadronic phase of nucleons and nuclei is only metastable would be almost inescapable, which would have far-reaching consequences for laboratory nuclear physics, the early universe, and astrophysical compact objects.

Acknowledgement: Supported by the Deutsche Forschungsgemeinschaft and by the Director, Office of Energy Research, Office of High Energy and Nuclear Physics, Division of Nuclear Physics, of the U.S. Department of Energy under Contract DE-AC03-76SF00098.

References

[1] R. N. Manchester and J. H. Taylor, *Pulsars*, W. H. Freeman and Co., San Francisco, 1977.

[2] D. C. Backer, S. R. Kulkarni, C. Heiles, M. M. Davis, and W. M. Goss, Nature **300** (1982) 615.

[3] R. N. Manchester, A. G. Lyne, C. Robinson, N. D'Amico, M. Bailes, and J. Lim, Nature **352** (1991) 219.

[4] N. K. Glendenning, Nucl. Phys. B (Proc. Suppl.) **24B** (1991) 110.

[5] J. L. Friedman, J. R. Ipser, and L. Parker, Astrophys. J. **304** (1986) 115.

[6] J. L. Friedman, J. R. Ipser, and L. Parker, Phys. Rev. Lett. **62** (1989) 3015.

[7] J. M. Lattimer, M. Prakash, D. Masak and A. Yahil, Astrophys. J. **355** (1990) 241.

[8] F. Weber, N. K. Glendenning, and M. K. Weigel, Astrophys. J. **373** (1991) 579.

[9] F. Weber and N. K. Glendenning, Astrophys. J. **390** (1992) 541.

[10] F. Weber and N. K. Glendenning, *Hadronic Matter and Rotating Relativistic Neutron Stars*, in: Proceedings of the International Summer School on Nuclear Astrophysics, Tianjin, China, June 17-27, 1991, to be published by World Scientific Publishing Company.

[11] E. Witten, Phys. Rev. D **30** (1984) 272.

[12] C. Alcock, E. Farhi and A. V. Olinto, Astrophys. J. **310** (1986) 261.

[13] P. Haensel, J. L. Zdunik, and R. Schaeffer, Astron. Astrophys. **160** (1986) 121.

[14] D. W. L. Sprung, Adv. Nucl. Phys. **5** (1972) 225.

[15] B. D. Day, Rev. Mod. Phys. **51** (1979) 821.

[16] V. R. Pandharipande and R. B. Wiringa, Rev. Mod. Phys. **51** (1979) 821.

[17] R. B. Wiringa, V. Fiks, and A. Fabrocini, Phys. Rev. C **38** (1988) 1010.

[18] P. C. Martin and J. Schwinger, Phys. Rev. **115** (1959) 1342.

[19] M. K. Weigel and G. Wegmann, Fortschr. Phys. **19** (1971) 451.

[20] L. Wilets, Green's functions method for the relativistic field theory many-body problem, in *Mesons in nuclei*, Vol. III, ed. M. Rho, D. Wilkinson, North-Holland, Amsterdam, 1979.

[21] R. Machleidt, K. Holinde, and Ch. Elster, Phys. Rep. **149** (1987) 1.

[22] K. Holinde, K. Erkelenz, and R. Alzetta, Nucl. Phys. **A194** (1972) 161; **A198** (1972) 598.

[23] P. Poschenrieder and M. K. Weigel, Phys. Lett. **200B** (1988) 231;
P. Poschenrieder and M. K. Weigel, Phys. Rev. C **38** (1988) 471.

[24] F. Weber and M. K. Weigel, Z. Phys. A**330** (1988) 249.

[25] F. Weber and M. K. Weigel, Nucl. Phys. **A505** (1989) 779, and references contained therein.

[26] B. D. Serot and J. D. Walecka, Adv. Nucl. Phys. **16** (1986) 1.

[27] C. J. Horowitz and B. D. Serot, Nucl. Phys. **A464** (1987) 613.

[28] F. Weber and M. K. Weigel, J. Phys. G **15** (1989) 765.

[29] N. K. Glendenning, Astrophys. J. **293** (1985) 470.

[30] N. K. Glendenning, Nucl. Phys. **A493** (1989) 521.

[31] H. A. Bethe and M. Johnson, Nucl. Phys. **A230** (1974) 1.

[32] V. R. Pandharipande, Nucl. Phys. **A178** (1971) 123.

[33] F. Weber, Habilitation Thesis, University of Munich, Munich, F.R.G., 1992.

[34] N. K. Glendenning, Phys. Rev. D **46** (1992) 1274.

[35] N. K. Glendenning, F. Weber, and S. A. Moszkowski, Phys. Rev. C **45** (1992) 844, (LBL-30296).

[36] N. K. Glendenning, Phys. Rev. Lett. **57** (1986) 1120.

[37] B. Friedman and V. R. Pandharipande, Nucl. Phys. **A361** (1981) 502.

[38] V. R. Pandharipande and R. B. Wiringa, Nucl. Phys. **A449** (1986) 219.

[39] R. B. Wiringa, R.A. Smith, and T. L. Ainsworth, Phys. Rev. C **29** (1984) 1207.

[40] I. E. Lagaris and V. R. Pandharipande, Nucl. Phys. **A359** (1981) 349.

[41] W. D. Myers, *Droplet Model of Atomic Nuclei* (New York: McGraw Hill, 1977);
W. D. Myers and W. Swiatecki, Ann. of Phys. **55** (1969) 395;
W. D. Myers and K.-H. Schmidt, Nucl. Phys. **A410** (1983) 61.

[42] P. K. Banerjee and D. W. L. Sprung, Can. J. Phys. **49** (1971) 1871.

[43] C. Mahaux, *Brueckner Theory of Infinite Fermi Systems*, Lecture Notes in Physics, Vol. 138, (Springer Verlag, Berlin, 1981).

[44] E. O. Fiset and T. C. Foster, Nucl. Phys. **A184** (1972) 588.

[45] Q. Ho-Kim and F. C. Khanna, Ann. Phys. **86** (1974) 233.

[46] F. Weber and M. K. Weigel, Phys. Rev. C **32** (1985) 2141.

[47] F. Coester, S. Cohen, B. Day, and C. M. Vincent, Phys. Rev. C **1** (1970) 769.

[48] C. W. Wong, Ann. Phys. (N. Y.) **72** (1972) 107.

[49] L. S. Celenza and C. M. Shakin, Phys. Rev. C **24** (1981) 2704.

[50] L. S. Celenza and C. M. Shakin, *Relativistic Nuclear Structure Physics*, World Scientific Lecture Notes in Physics, Vol. 2, World Scientific, Singapore, 1986.

[51] B. ter Haar and R. Malfliet, Phys. Rev. Lett. **59** (1987) 1652.

[52] F. Weber and N. K. Glendenning, Phys. Lett. **265B** (1991) 1.

[53] H. Heiselberg, C. J. Pethick, and E. F. Staubo, *Quark Matter Droplets in Neutron Stars*, NORDITA preprint 92/39A, submitted to Phys. Rev. Lett. (1992).

[54] N. K. Glendenning, *Supernovae, Compact Stars and Nuclear Physics*, invited paper in Proc. of 1989 Int. Nucl. Phys. Conf., Sao Paulo, Brasil, Vol. 2, ed. by M. S. Hussein et al., World Scientific, Singapore, 1990.

[55] N. K. Glendenning, *Strange-Quark-Matter Stars*, in: Proc. Int. Workshop on Relativ. Aspects of Nucl. Phys., ed. by T. Kodama, K. C. Chung, S. J. B. Duarte, and M. C. Nemes, World Scientific, Singapore, 1990.

[56] J. Ellis, J. I. Kapusta, and K. A. Olive, Nucl. Phys. **B348** (1991) 345.

[57] G. Baym and S. Chin, Phys. Lett. **62B** (1976) 241.

[58] B. D. Keister and L. S. Kisslinger, Phys. Lett. **64B** (1976) 117.

[59] G. Chapline and M. Nauenberg, Phys. Rev. D **16** (1977) 450.

[60] W. B. Fechner and P. C. Joss, Nature **274** (1978) 347.

[61] H. A. Bethe, G. E. Brown, and J. Cooperstein, Nucl. Phys. **A462** (1987) 791.

[62] B. D. Serot and H. Uechi, Ann. Phys. (N. Y.) **179** (1987) 272.

[63] W. D. Arnett and R. L. Bowers, Astrophys. J. Suppl. **33** (1977) 415.

[64] J. H. Taylor and J. M. Weisberg, Astrophys. J. **345** (1989) 434.

[65] S. A. Rappaport and P. C. Joss, *Accrection Driven Stellar X-Ray Sources*, ed. by W. H. G. Lewin and E. P. J. van den Heuvel, Cambridge University Press, 1983.

[66] F. Nagase, Publ. Astron. Soc. Japan **41** (1989) 1.

[67] N. K. Glendenning, *Nuclear and Particle Astrophysics*, Proc. Int. Summer School on the Structure of Hadrons and Hadronic Matter, Dronton, Netherlands, August 5-18, 1990, World Scientific, Singapore (LBL-29415).

[68] J. Van Paradijs, Astrophys. J. **234** (1978) 609.

[69] S. L. Shapiro and S. A. Teukolsky, *Black Holes, White Dwarfs, and Neutron Stars*, John Wiley & sons, N. Y., 1983.

[70] M. Y. Fujimoto and R. E. Taam, Astrophys. J. **305** (1986) 246.

[71] M. Rudermann, Ann. Rev. Astr. Ap. **10** (1972) 427.

[72] G. Baym and C. Pethick, Ann. Rev. Nucl. Sci. **25** (1975) 27.

[73] V. Trimble and M. Rees, Astrophys. Lett. **5** (1970) 93.

[74] G. Borner and J. M. Cohen, Astrophys. J. **185** (1973) 959.

[75] E. P. Liang, Astrophys. J. **304** (1986) 682.

[76] K. Brecher and A. Burrows, Astrophys. J. **240** (1980) 642.

[77] R. Ramaty and P. Meszaros, Astrophys. J. **250** (1981) 384.

[78] M. A. Ruderman, Nature **223** (1969) 597.

[79] G. Baym and D. Pines, Ann. Phys. (N.Y.) **66** (1971) 816.

[80] J. D. Alonso and J. H. Ibanez Cabanell, Astrophys. J. **291** (1985) 308.

[81] R. Ruffini, in *Physics and Astrophysics of Neutron Stars and Black Holes* (North Holland, Amsterdam, 1978) p. 287.

[82] N. K. Glendenning and F. Weber, *Nuclear Solid Crust on Rotating Strange Stars* (LBL-31613) (to appear in The Astrophys. Journal).

[83] L. Lindblom, Astrophys. J. **303** (1986) 146.

[84] L. Lindblom, *Instabilities in Rotating Neutron Stars*, in The Structure and Evolution of Neutron Stars, Proceedings, ed. by D. Pines, R. Tamagaki, and S. Tsuruta, Addison-Wesley, 1992.

[85] F. Weber and N. K. Glendenning, Z. Phys. **A339** (1991) 211.

[86] R. F. Sawyer, Phys. Rev. D **39** (1989) 3804.

[87] J. R. Ipser and L. Lindblom, Astrophys. J. **355** (1990) 226.

[88] J. R. Ipser and L. Lindblom, Astrophys. J. **373** (1991) 213.

[89] F. Weber and N. K. Glendenning, *Impact of the Nuclear Equation of State on Models of Rotating Neutron Stars*, Proc. of the Int. Workshop on Unstable Nuclei in Astrophysics, Tokyo, Japan, June 7-8, 1991, Eds. S. Kubono and T. Kajino, World Scientific, 1992.

[90] N. K. Glendenning, *Limiting Rotational Period of Neutron Stars* (LBL-31511) (to appear in the 15 November 1992 issue of Phys. Rev. D).

[91] N. K. Glendenning, Mod. Phys. Lett. **A5** (1990) 2197.

[92] F. Weber and N. K. Glendenning, *Interpretation of Rapidly Rotating Pulsars*, in: Proceedings of the Second International Symposium on Nuclear Astrophysics, NUCLEI IN THE COSMOS, Karlsruhe, Germany, July 6-10, 1992, to appear in The Journal of Physics (England), (LBL-32562).

[93] J. Madsen and M. L. Olesen, Phys. Rev. D **43** (1991) 1069, ibid., **44**, 4150 (erratum).

[94] R. R. Caldwell and J. L. Friedman, Phys. Lett. **264B** (1991) 143.

[95] G. Baym, C. Pethick, and P. Sutherland, Astrophys. J. **170** (1971) 299.

[96] P. Pizzochero, Phys. Rev. Lett. **66** (1991) 2425.

List of Figures

List of Tables

LAWRENCE BERKELEY LABORATORY
UNIVERSITY OF CALIFORNIA
TECHNICAL INFORMATION DEPARTMENT
BERKELEY, CALIFORNIA 94720